Heat Flow Parameters Affecting Dendrite Spacings during Unsteady-State Solidification of Sn-Pb and Al-Cu Alloys

OTÁVIO L. ROCHA, CLÁUDIO A. SIQUEIRA, and AMAURI GARCIA

Solidification thermal parameters and dendrite arm spacings have been measured in hypoeutectic Sn-Pb and Al-Cu alloys solidified under unsteady-state heat flow conditions. It was observed that both primary and secondary spacings decreased with increased solute content for Sn-Pb alloys. For Al-Cu alloys, the primary spacing was found to be independent of composition, and secondary spacings decrease as the solute content is increased. The predictive theoretical models for primary spacings existing in the literature did not generate the experimental observations concerning the Sn-Pb and Al-Cu alloys examined in the present study. The theoretical Bouchard–Kirkaldy's (BK's) equation relating secondary spacings with tip growth rate has generated adequately the experimental results for both metallic systems. The insertion of analytical expressions for tip growth rate and cooling rate into the predictive model, or into the resulting experimental equations in order to establish empirical formulas permitting primary and secondary dendritic spacings to be determined as functions of unsteady-state solidification parameters such as melt superheat, type of mold, and transient metal/mold heat-transfer coefficient is proposed.

I. INTRODUCTION

DURING solidification of alloys, the observed microstructures are diverse, but in general can be classified into two basic groups: cells/dendrites and eutectic morphologies. Dendrite growth is the common mechanism of crystallization from metallic melts, and the morphology, which is formed, consists of an array of dendrites with a sidebranch configuration. The solute, which is redistributed due to the solubility difference between the solid and liquid phases, provokes an important consequence of such a structure, *i.e.*, the occurrence of microsegregation between the dendrites branches. The dendritic array characterized by primary and secondary spacings and the segregated products greatly affect the mechanical properties and homogenization kinetics of solidified alloys.[1,2] Therefore, in order to control the properties of casting materials, it is important to understand the solidification parameters that affect the growth of dendritic spacings during solidification.

Numerous directional solidification studies have been reported with a view to characterizing primary (λ_1) and secondary (λ_2) dendrite arm spacings as a function of alloy solute concentration (C_0), tip growth rate (V_L), and temperature gradient ahead of the macroscopic solidification front (G_L).[1–54] A recent article by Bouchard and Kirkaldy[29] has summarized these studies grouped into two categories: those involving solidification in steady-state heat flow and those in unsteady-state regime. In the former category, solidification is controlled and the significant controllable variables, G_L and V_L, are maintained constant and are practically independent of each other. In the latter, which characterizes,

for instance, the solidification conditions of a body of irregular shape, these variables are interdependent, cannot be controlled, and vary freely with time. The analysis of dendritic structures in the unsteady-state regime is very important, since it encompasses the majority of industrial solidification processes.

The measurements of primary and secondary dendrite arm spacings involve looking at the microstructure after complete solidification. Primary spacings do not coarsen with time and can be accurately measured from the microstructure and compared with growth models. On the other hand, secondary spacings are seen to rapidly coarsen during solidification, and the effect of coarsening has to be taken into account by the predictive growth models.[29] Most of the results in the literature, concerning steady and unsteady regimes, pertaining to λ_2 in hypoeutectic alloys, indicate a decrease in spacing with increasing cooling rate for a given alloy composition and with increasing solute content for a given cooling rate.[28,29,38,39] The reports in the literature also indicate that for steady or unsteady growth conditions, the primary arm spacings decrease as G_L or V_L increases.[1–54] On the other hand, there has been some disagreement in the literature regarding the influence of the initial alloy composition on primary spacings. It has been reported in the majority of cases that λ_1 increases as C_0 (for hypoeutetic alloys) increases for both steady and unsteady growth conditions.[28,29] However, Sharp and Hellawell[44] found that C_0 has little effect on primary spacings and Spittle and Lloyd[46] reported that for steady-state growth with low G_L, λ_1 decreased as C_0 increased and was independent of C_0 for high G_L, and for unsteady solidification λ_1 decreased as C_0 increased.

The present article focuses on the dependence of dendrite arm spacings on solidification thermal parameters, *i.e.*, dendrite tip growth rate, temperature gradient in front of the liquidus isotherm, and tip cooling rate, and on the alloy solute content under unsteady-state solidification conditions. The experimental data concerning the solidification

OTÁVIO L. ROCHA and CLÁUDIO A. SIQUEIRA, Doctorate Students and Research Assistants, and AMAURI GARCIA, Professor, are with the Department of Materials Engineering, State University of Campinas—Unicamp, 13083-970 Campinas-SP, Brazil. Contact e-mail: amaurig @fem.unicamp.br

of Sn 5, 15, and 30 wt pct Pb and Al 5, 8, and 15 wt pct Cu alloys, directionally solidified under different conditions of heat-transfer efficiency at the metal/mold interface, are compared with theoretical predictions furnished by models from the literature. The use of an analytical solidification model, coupled with predictive dendritic growth models or empirical dendritic growth equations, in order to permit the dendrite spacings to be directly correlated with solidification processing variables such as the transient metal/mold heat-transfer coefficient, melt superheat, and metal and mold thermophysical characteristics is proposed.

II. DENDRITIC SPACING MODELS AND ANALYTICAL SOLIDIFICATION THERMAL PARAMETERS

A. Dendritic Spacing Models

Several important theoretical[1–25] and experimental[26–53] studies have been developed, with the objective of selecting primary and secondary dendritic spacings. Among the theoretical models existing in the literature, only those proposed by Hunt and Lu[4] for primary spacings and Bouchard and Kirkaldy[29] for primary and secondary spacings assume solidification in unsteady-state heat flow conditions. Hunt,[1] Kurz and Fisher,[2,3] and Trivedi[21] have derived primary spacing formulas, which apply for steady-state conditions. The theoretical models for determination of dendritic spacings proposed by these authors are shown in Eqs. [1] through [8]:

$$\lambda_1 = 2.83[\Gamma m_L C_0 (1 - k_0) D]^{1/4} G_L^{-1/2} V_L^{-1/4}$$
$$\text{(Hunt, cellular/dendritic)} \quad [1]$$

$$\lambda_1 = 4.3 \left(\frac{\Gamma \Delta T D}{k_0} \right)^{1/4} G_L^{-1/2} V_L^{-1/4}$$
$$\text{(Kurz and Fisher, cellular/dendritic)} \quad [2]$$

$$\lambda_1 = 2.83[L\Gamma m_L C_0 (1 - k_0) D]^{1/4} G_L^{-1/2} V_L^{-1/4}$$
$$\text{(Trivedi, dendritic)} \quad [3]$$

$$\lambda'_1 = 0.07798 \, V'^{(a-0.75)} (V' - G')^{0.75} G'^{-0.6028}$$
$$\text{(Hunt and Lu (HL), dendritic)} \quad [4]$$

where

$$a = -1.131 - 0.1555 \log_{10} (G')$$
$$- 0.007589 [\log_{10} (G')]^2 \quad [5]$$

$$\lambda'_1 = \frac{\lambda_1 \Delta T}{\Gamma k_0}, \, G' = \frac{G_L \Gamma k_0}{\Delta T^2} \text{ and } V' = \frac{V_L \Gamma k_0}{D \Delta T} \quad [6]$$

$$\lambda_1 = a_1 \left(\frac{16 C_0^{1/2} G_0 \varepsilon \Gamma D}{(1 - k_0) m_L G_L V_L} \right)^{1/2}$$
$$\text{(Bouchard-Kirkaldy (BK) primary dendritic)} \quad [7]$$

where λ_1 is the primary dendritic spacing, Γ is the Gibbs–Thomson coefficient, m_L is the liquidus line slope, k_0 is the solute partition coefficient, C_0 is the alloy composition, D is the liquid solute diffusivity, ΔT is the difference between the liquidus and solidus equilibrium temperature, V_L is the

dendrite tip growth rate, G_L is the temperature gradient in front of the liquidus isotherm, $G_0 \varepsilon$ is a characteristic parameter $\approx 600 \times 6$ K cm^{-1},[29] and a_1 is the primary dendrite calibrating factor. Since the spacings proposed by Hunt and Lu (Eqs. [4] through [6]) refer to the radius rather than to the more commonly measured diameter and they are minimum spacings, the values need to be multiplied by 2 to 4 for comparison with measured spacings.

The Trivedi model[21] is a result of a Hunt's model modification, where L is a constant that depends on harmonic perturbations. According to Trivedi, for dendritic growth, L is equal to 28.

For secondary dendrite spacings, Bouchard and Kirkaldy[29] derived an expression, which is very similar to the Mullins, and Sekerka,[57,58] temperature gradient–independent marginal wavelength formula, which is given by

$$\lambda_2 = 2\pi a_2 \left(\frac{4\Gamma}{C_0 (1 - k_0)^2 T_F} \left(\frac{D}{V_L} \right)^2 \right)^{1/3} \quad [8]$$

where a_2 is the secondary dendrite-calibrating factor, which depends on the alloy composition and T_F is the fusion temperature of the solvent.

B. Solidification Thermal Parameters

In order to determine the solidification thermal parameters such as the tip growth rate, the thermal gradient in the liquid immediately at the right of the tip interface, and the cooling rate, an analytical model is applied to simulate the solidification of binary alloys in a cylindrical cavity chilled from below. The model employs the mathematically expedient technique of replacing the interfacial thermal resistance by equivalent layers of material in a virtual system, and the latent heat of fusion is taken into account by adjusting the specific heat over the solidification temperature range.[40,55] The ingot is treated as a one-dimensional moving boundary problem in which boundaries at the tips and roots of the dendrites are simultaneously considered. It is assumed that the Newtonian interface resistance is represented by a metal/mold heat-transfer coefficient h_i. The other thermophysical properties describing the system are treated as averages within the same phase, as follows:

Liquid	$T > T_{\text{Liq}}$	K_L, ρ_L, c_L [9]
Mushy	$T_{\text{Sol}} < T < T_{\text{Liq}}$	$K_{SL} = (K_S + K_L)/2$ [10]
		$\rho_{SL} = (\rho_S + \rho_L)/2$ [11]
		$c_{SL} = c_L + L/(T_{\text{Liq}} - T_{\text{Sol}})$ [12]
Solid	$T < T_{\text{Sol}}$	K_S, ρ_S, c_S [13]

where K is the thermal conductivity, c is the specific heat, ρ is the density, L is the latent heat of fusion, T_{Liq} is the liquidus temperature, T_{Sol} is the nonequilibrium solidus temperature, and subscripts S, SL, and L represent the solid, mushy, and liquid metal, respectively.

The one-dimensional Fourier field equation is exactly applicable to the virtual metal/mold system, and the solution obtained in the system can be related to the real system by simple relationships. The model has been detailed in previ-

ous articles and validated against experimental data describing the unidirectional solidification of Al-Cu[40] and Zn-Al[55] alloys. The temperature gradient and the growth rate at the dendrite tips are given, respectively, by

$$G_L = \left[\frac{m(T_p - T_{\text{Liq}})}{\sqrt{\pi} \cdot \alpha_{SL}\phi_2[1 - \text{erf}(m\phi_2)]\exp(m\phi_2)^2} \right] \cdot$$

$$\frac{2\alpha_{SL}\phi_2^2}{\left[\dfrac{2K_S\phi_2(T_{\text{Sol}} - T_0)}{n\sqrt{\pi}(T_{\text{Liq}} - T_0)\exp(\phi_1^2)[M + \text{erf}(\phi_1)]h_i} \right] + S_L} \quad [14]$$

$$V_L = \frac{2\alpha_{SL}\phi_2^2}{\left[\dfrac{2\,K_S\,\phi_2\,(T_{\text{Sol}} - T_0)}{n\sqrt{\pi}\,(T_{\text{Liq}} - T_0)\exp(\phi_1^2)\,[M + \text{erf}(\phi_1)]\,h_i} \right] + S_L} \quad [15]$$

By multiplying Eqs. [14] and [15], the individual effects of alloy composition, melt superheat ($\Delta T_p = T_p - T_{\text{Liq}}$), and metal/mold heat-transfer coefficient (h_i) can be seen inserted into an expression correlating tip cooling rate ($\dot{T}_L$) and solidification parameters, given by

$$\dot{T}_L = \left[\frac{m\Delta T_p}{\sqrt{\pi} \cdot \alpha_{SL}\phi_2[1 - \text{erf}(m\phi_2)]\exp(m\phi_2)^2} \right]$$

$$\left[\frac{2\alpha_{SL}\phi_2^2}{\dfrac{2K_S\phi_2(T_{\text{Sol}} - T_0)}{n\sqrt{\pi}(T_{\text{Liq}} - T_0)\exp(\phi_1^2)[M + \text{erf}(\phi_1)]h_i} + S_L} \right] \quad [16]$$

where m is the square root of the ratio of thermal diffusivities of mushy zone and liquid $(\alpha_{SL}/\alpha_L)^{1/2}$, α_L is the liquid thermal diffusivity ($K_L/c_L\rho_L$), T_0 is the environment temperature, T_p is the pouring temperature, n is the square root of the ratio of thermal diffusivities of solid and mushy zone, M is the ratio of heat diffusivities of solid and mold material, and S_L is the position of liquidus isotherm from metal/mold interface. Solidification constants ϕ_1 and ϕ_2 are associated with the displacement of solidus and liquidus isotherms, and can be determined by the simultaneous solution of the following equations:

$$\frac{(T_{\text{Liq}} - T_{\text{Sol}})}{\text{erf}(\phi_2) - \text{erf}(n\phi_1)} = \frac{K_S \exp[(n^2 - 1)\phi_1^2]}{K_{SL}n[M + \text{erf}(\phi_1)]}(T_{\text{Sol}} - T_0) \quad [17]$$

$$\frac{(T_{\text{Liq}} - T_{\text{Sol}})}{\text{erf}(\phi_2) - \text{erf}(n\phi_1)} = \frac{K_L m \exp[(1 - m^2)\phi_2^2]}{K_{SL}[1 - \text{erf}(m\phi_2)]}(T_p - T_{\text{Liq}}) \quad [18]$$

III. EXPERIMENTAL PROCEDURE

The casting assembly used in solidification experiments has been detailed in a previous article.[59] The heat was extracted through a water-cooled bottom, promoting upward directional solidification. A stainless steel mold was used, having an internal diameter of 50 mm, height 110 mm, and wall thickness of 5 mm. The inner vertical surface was covered with a layer of insulating alumina to minimize radial heat losses, and a top cover made of an insulating material was used to reduce heat losses from the metal/air surface. The bottom part of the mold was closed with a thin (3 mm) carbon steel sheet. In some experiments with Sn-Pb alloys, these steel sheets were coated with an alumina-based mold wash in order to reduce the metal/mold heat-transfer efficiency (permitting investigation of the influence of a lower range of cooling rates on the dendritic array). The mold wash was applied to the internal surface of the steel sheets with a spray gun, with the coating film thickness standardized at about 100 μm. The alloys were melted *in situ* and the lateral electric heaters had their power controlled in order to permit a desired superheat to be achieved. To begin solidification, the electric heaters were disconnected and at the same time the water flow was initiated.

Experiments were performed with Sn-Pb alloys (5, 15, and 30 wt pct Pb) and Al-Cu alloys (5, 8, and 15 wt pct Cu). The chemical composition of metals that were used to prepare these alloys are presented in Table I. Starting melt superheats were standardized at 1.1 times the liquidus temperature. The thermophysical properties of these alloys are summarized in Table II.

Continuous temperature measurements in the casting were monitored during solidification *via* the output of a bank of fine type-K thermocouples sheathed in 1.6-mm-diameter steel tubes, and positioned at 5, 10, 15, 30, and 50 mm from the heat-extracting surface at the bottom of the crucible. The thermocouples were calibrated at the melting point of tin (for Sn-Pb alloys) and aluminum (for Al-Cu alloys) exhibiting fluctuations of about 0.4 °C and 1 °C, respectively. All of the thermocouples were connected by coaxial cables to a data logger interfaced with a computer, and the temperature data were acquired automatically.

Selected transverse and longitudinal sections of the directionally solidified specimens at 5, 10, 15, 20, 30, 40, 50, 60, and 70 mm from the metal/mold interface were electropolished and etched with acid solutions (50 ml glycerin, 35 ml acetic acid, and 15 ml of HNO$_3$, 38 °C to 40 °C for Sn-Pb alloys, and NaOH 5 pct for Al-Cu alloys) for microscopic examination.

The method used for measurement of the primary dendrite arm spacings on the transverse section (perpendicular to the growth direction) was the triangle method.[38,39] The

Table I. Chemical Analyses of Metals Used to Prepare Al-Cu and Sn-Pb Alloys

Metal	Chemical Compositions (Wt Pct)									
	Fe	Ni	Cu	Si	Mg	Pb	Cr	Mn	Zn	Sn
Al	0.182	0.0148	0.0242	0.103	0.0013	—	—	—	—	—
Cu	—	—	—	0.09	—	0.002	0.27	—	—	—
Sn	0.009	—	0.007	—	—	0.19	—	0.0025	—	—
Pb	0.002	0.003	—	—	—	—	—	—	0.003	0.25

Table II. Casting Materials Used for Experimentation and the Corresponding Thermophysical Properties[29,40]

Properties	Symbol/ Units	Sn-5 Wt Pct Pb	Sn-15 Wt Pct Pb	Sn-30 Wt Pct Pb	Al-5 Wt Pct Cu	Al-8 Wt Pct Cu	Al-15 Wt Pct Cu
Thermal conductivity	K_s (W/m · K) (solid)	65.6	62.5	57.4	192	188.4	179.1
	K_L (W/m · K) (liquid)	32.8	32.5	32	88.8	86.9	82.5
Specific heat	c_s (J/kg · K) (solid)	217	208	194	1,090	1,087.7	1,082.5
	c_L (J/kg · K) (liquid)	253	241	223	1,056.7	1,039.3	999
Density	ρ_s(kg/m^3) (solid)	7,475	7,867	8,495.2	2,667	2,745.6	2,929
	ρ_L (kg/m^3) (liquid)	7,181	7,552	8,085.4	2,501	2,580	2,763.8
Latent heat of fusion	L (J/kg)	59,214	55,861	50,499	381,415	379,264	374,245
Solute diffusivity	D (m^2/s)	4.5×10^{-9}	4.5×10^{-9}	4.5×10^{-9}	3.5×10^{-9}	3.5×10^{-9}	3.5×10^{-9}
Gibbs–Thomson coefficient	Γ (m · K)	6.65×10^{-8}	6.52×10^{-8}	6.41×10^{-8}	15.2×10^{-8}	14.7×10^{-8}	13.6×10^{-8}
Fusion temperature	T_F (°C) solvent	232	232	232	660	660	660
Solidus temperature	T_{Sol} (°C)	183	183	183	548	548	548
Liquidus temperature	T_{Liq} (°C)	226	213	193	643	633	609
Partition coefficient	k_0	0.0656	0.0656	0.0656	0.17	0.17	0.17
Liquidus slope	m_L (K/wt pct)	−1.3	−1.3	−1.3	−3.4	−3.4	−3.4
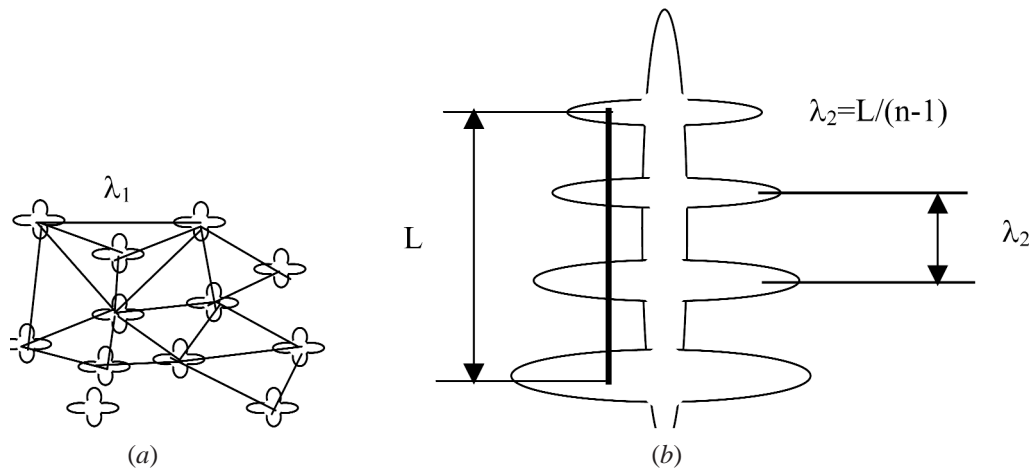
Fig. 1—Schematic representation of methods used for measurement of (*a*) primary and (*b*) secondary dendrite arm spacings.

triangle is formed by joining the three neighboring dendrite centers, the sides of the triangle corresponding to λ_1, as shown in Figure 1(a). Values for λ_2 were measured by averaging the distance between adjacent side branches on the longitudinal section of a primary dendrite as a function of the distance from the dendrite tip, as shown in Figure 1(b). In these methods 40 λ_1 and λ_2 values were measured for each selected position from metal/mold interface.

Image processing systems Neophot 32 (Carl Zeiss, Esslingen, Germany) and Leica Quantimet 500 MC (Leica Imaging systems Ltd., Cambridge, England) were used to measure dendrites spacings and their distribution range.

IV. RESULTS AND DISCUSSION

A typical example of the experimental cooling curves for the five thermocouples inserted into the casting, during solidification of a Sn 5 wt pct Pb alloy, is shown in Figure 2. The temperature files containing the experimentally monitored temperatures were used in a finite-difference heat flow program to determine the transient metal/coolant heat-transfer coefficient, h_i, by using a technique described in a previous article.[56] Figure 3 shows the time dependence of h_i during the course of different experiments of upward directional solidification of Al-Cu and Sn-Pb alloys in un-
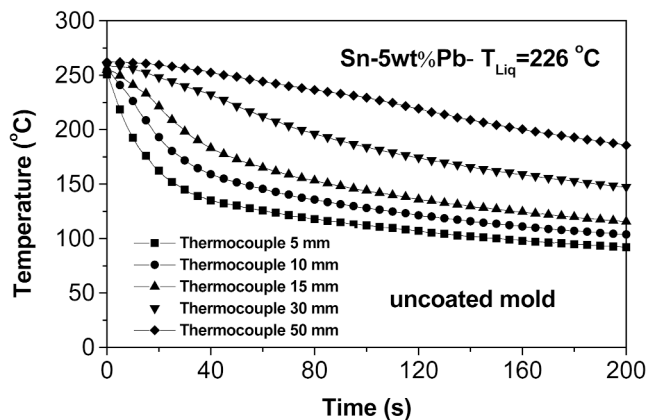
Fig. 2—Experimental cooling curves for the five thermocouples inside the casting. Curves are for thermocouples at 5, 10, 15, 30, and 50 mm from the metal/mold interface.
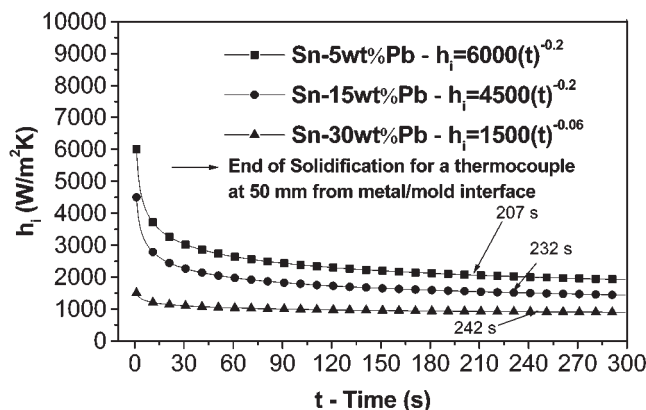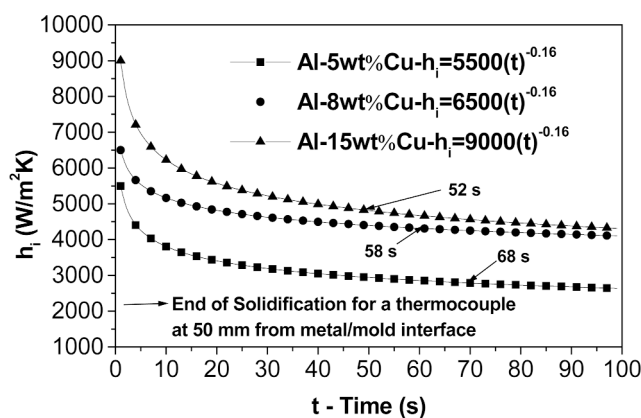

Fig. 3—Evolution of metal-mold interface heat-transfer coefficients as a function of time for Al-Cu and Sn-Pb alloys during vertical upward solidification in uncoated cooled molds.

coated molds. The corresponding values for Sn-Pb alloys solidified in coated molds are shown in Figure 4(a). In order to investigate the difference on h_i profiles during vertical and horizontal directional solidification, an experiment of horizontal directional solidification has been performed with a Sn 5 wt pct Pb alloy, under the same conditions of metal superheat and mold surface condition (uncoated mold). Figure 4(b) shows the experimental h_i profiles for both cases. It can be seen that, except for the initial values, the profiles are very close, and during most of the solidification process, similar

h_i values are operative. The initial difference can be explained by the differences in the physical configuration of the two experimental setups. In the horizontal setup, the measured h_i is a metal/mold heat-transfer coefficient, while in the vertical configuration, h_i is the overall Metal/Coolant heat-transfer coefficient, i.e., it encompasses also the thermal resistance of the 3-mm-thick steel sheet used as the mold bottom as well as the water/mold thermal resistance. The heat-transfer coefficients expressed as a power function of time have been used by the analytical model in order to provide theoretical predictions for tip growth rate (V_L) and tip cooling rate $\dot{T}_L$.

The experimental results of thermal analysis in metal have also been used to determine the displacement of liquidus isotherm, as well as tip growth rate, as a function of time and position. Figure 5 show comparisons between experimental results and analytical predictions of V_L (Eq. [15]) for Sn-Pb and Al-Cu alloys, and a good agreement can be observed.

The cooling rate immediately after the passing of the liquidus front was computed by determining the slope of the experimental cooling curves. These values are compared in Figure 6 with theoretical predictions furnished by the analytical model and a fair to good agreement can be observed.

Values of G_L, necessary for calculating the theoretical predictions furnished by some spacing models, were determined from the experimental values of V_L and $\dot{T}_L$ ($\dot{T}_L = G_L V_L$).

Typical microstructures observed along the transverse and longitudinal sections of Sn 5, 15, and 30 wt pct Pb castings and Al 5, 8, and 15 wt pct Cu castings are shown in Figures 7 (a) and (b), respectively. Figures 8 and 9 present the mean experimental values of primary and secondary dendritic spacings as a function of cooling rate (primary) and tip growth rate (secondary), respectively, measured from the aforementioned microstructures. Points are experimental results and lines represent an empirical fit of the experimental points, with dendritic spacings being expressed as a power function either of tip growth rate or of tip cooling rate. It can be seen that the use of a water-cooled mold imposes higher values of tip growth rates and cooling rates near the casting surface and a decreasing profile along the casting due to the increasing thermal resistance of the solidified shell with distance from the cooled surface. This influence translates to the observed experimental values of primary and secondary dendritic spacings. It can be observed that a -0.55 power law characterizes the experimental variation of primary spacings with cooling rate (Figure 8). This is in good agreement with the observations of Bouchard and Kirkaldy,[29] which have concluded that in unsteady-state solidification, an exponential relationship $\lambda_1 = $ constant $(\dot{T})^{-0.50}$ best generates the existing experimental results. The analytical solidification expressions for the thermal gradient G_L and tip growth rate V_L (Eqs. [14] and [15], respectively) show that for unsteady-state solidification, G_L is coupled to the tip growth rate and can be related to V_L by an expression of the form $G_L = $ constant $\cdot (V_L)$, and consequently $\dot{T}_L = $ constant $\cdot (V_L)^2$. In this case, a -1.1 exponent would characterize experimental power laws concerning the variation of primary spacings with the tip growth rate. It can be seen in Figure 9 that a $-2/3$ power law characterizes the experimental variation of secondary spacings with tip growth rate. Although the experimental equations do not explicitly predict that the functional relationship of λ_2 with the cooling rate ($\dot{T}$) is $-1/3$, it is implicit from the linear relationship between V_L and G_L.
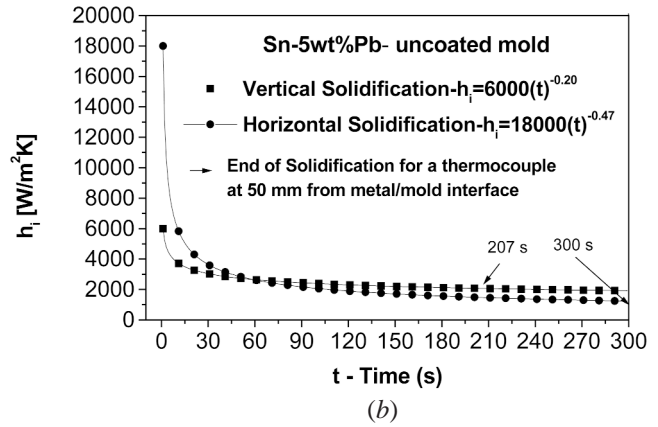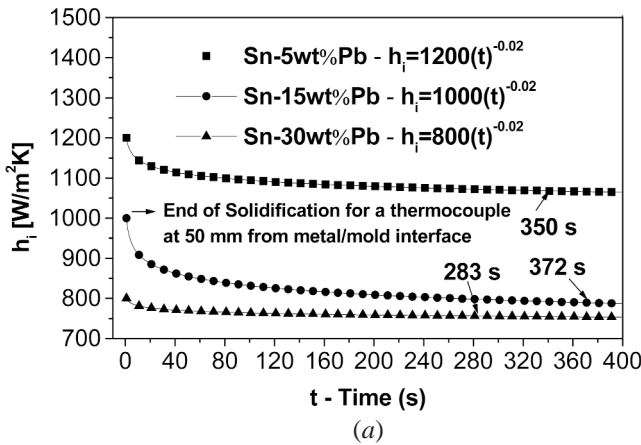
Fig. 4—Evolution of metal/mold heat-transfer coefficient as a function of time: (*a*) vertical upward solidification/coated mold and (*b*) vertical and horizontal directional solidification.
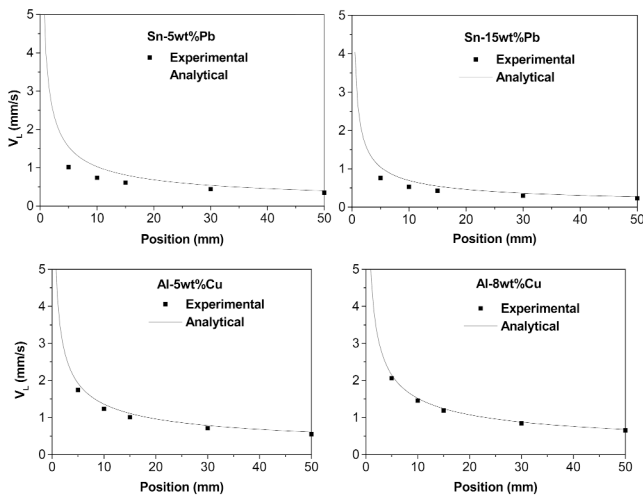

Fig. 5—Tip growth rate as a function of position from metal/mold interface for Sn-Pb and Al-Cu alloys during upward vertical solidification in uncoated cooled molds.
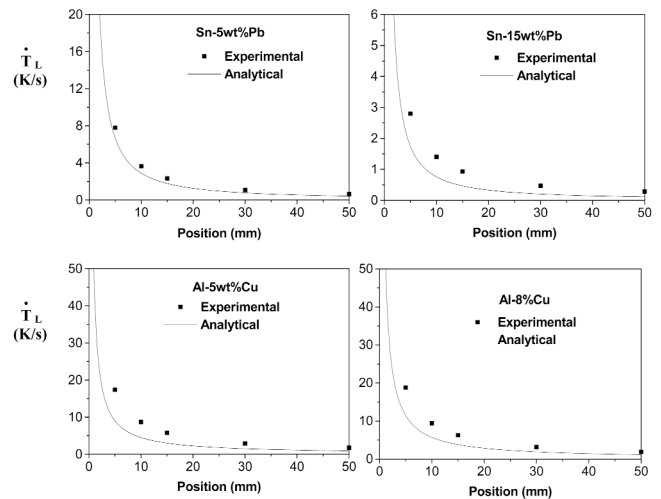

Fig. 6—Tip cooling rate as a function of position from metal/mold interface for Sn-Pb and Al-Cu alloys during upward vertical solidification in uncoated cooled molds.

During solidification, the primary spacing either remains constant with respect to time under steady-state growth or continuously readjusts in response to the changing conditions at the advancing solidification front under unsteady-state growth. There is little work in the literature investigating the effect of the solute content on λ_1 during unsteady-state solidification. In the present work, the influence of the initial alloy composition (C_0) on primary spacings can be examined by comparing the relative position of the experimental points in Figure 8(a). For Al-Cu alloys, C_0 is found to have little effect on λ_1 with a single power law representing the variation of spacings with tip growth rate for all three alloys examined. This is in good agreement with the observations reported by Sharp and Hellawell,[44] which found that the primary arm spacing is almost independent of composition. For Sn-Pb alloys, λ_1 is observed to decrease as C_0 is increased. A similar conclusion was reported by Spittle and Lloyd[46] based on experimental results of hypoeutectic Pb-Sb alloys directionally solidified under non-steady heat flow conditions at cooling rates of the same order of magnitude as those used in the present experiments for

Sn-Pb alloys. These results contradict the experimental/theoretical analysis by Okamoto and Kishitake,[28] in which the primary arm spacings increase with increasing solute content for unsteady-state heat flow solidification.

Figures 10 and 11 show comparisons between the present experimental results of primary spacings with theoretical predictions furnished by unsteady-state predictive models, for Sn-Pb and Al-Cu alloys, respectively. They are the HL's model, represented by Eqs [4] through [6], and BK's model, given by Eq.[7,] with calibration factors a_1 of 50 for Sn-Pb alloys and 250 for Al-Cu alloys, as suggested by these authors.[29] It can be seen in Figure 10 that both models overestimate the primary spacings, except for the alloy with the lowest solute content (Sn 5 wt pct Pb), where a good agreement can be observed. For Al-Cu alloys, HL's model underestimates the spacings and BK's model overestimates λ_1, for the three alloys experimentally examined, as shown in Figure 11.

The predicted dendritic spacings calculated for unsteady solidification by the HL and BK models are subjected to deviations caused mainly by the unaccounted diffusion
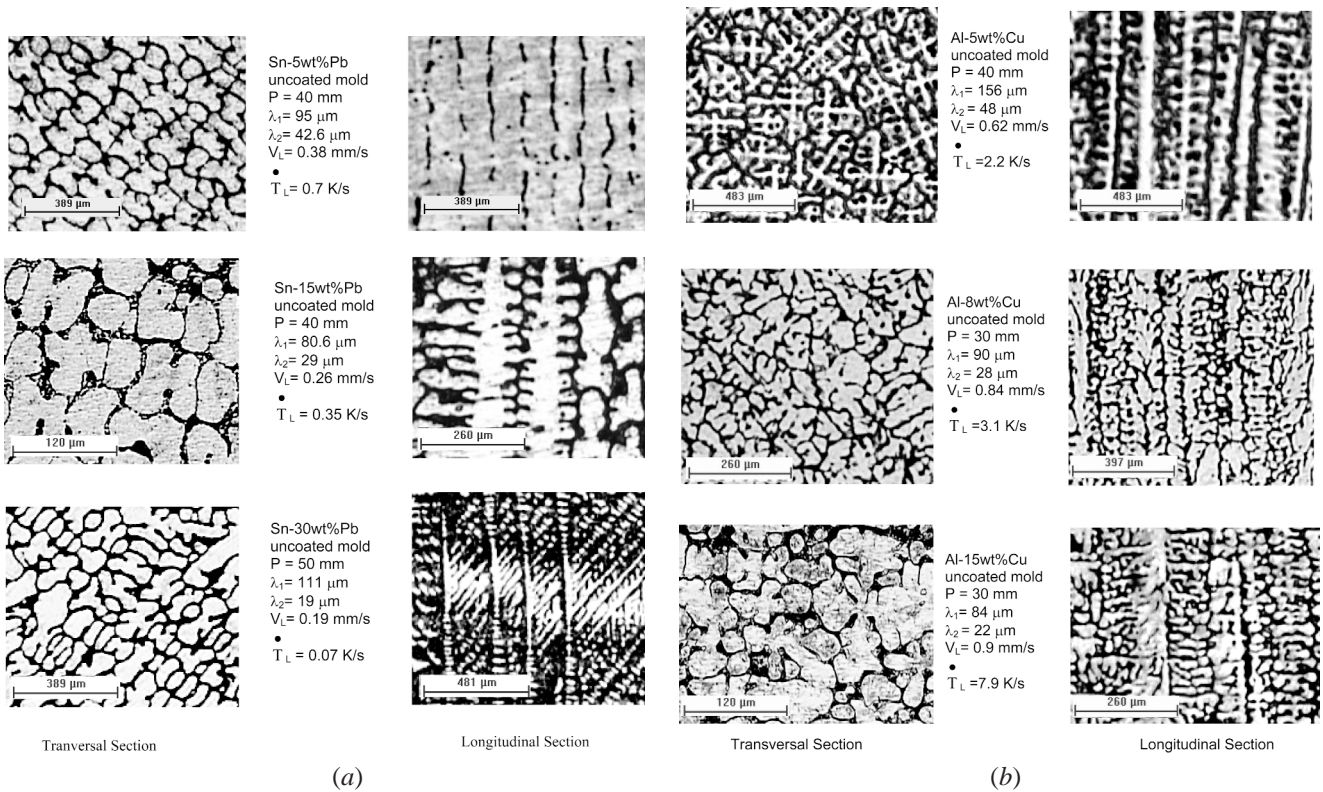
Fig. 7—(*a*) Solidification microstructures for Sn-Pb alloys. P is the position from the metal/mold interface. (*b*) Solidification microstructures for Al-Cu alloys. P is the position from metal/mold interface.
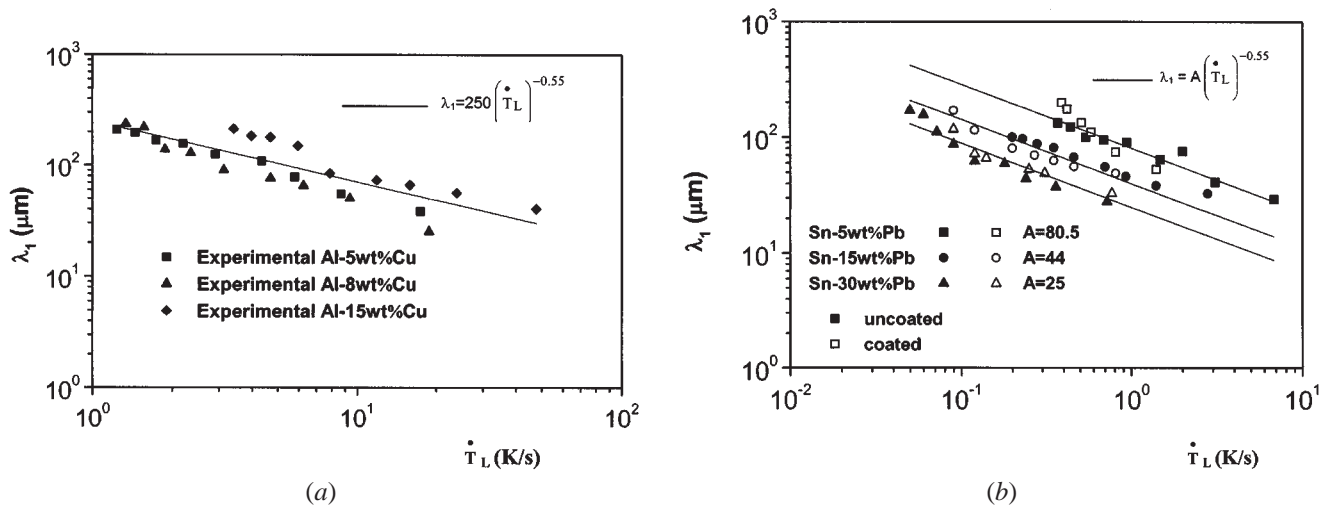

Fig. 8—Primary dendrite arm spacing as a function of cooling rate for (*a*) Al-Cu and (*b*) Sn-Pb alloys.

relaxations and coring reductions for primary spacings and Ostwald ripening for secondary spacings.[29] Other uncertainties such as thermophysical properties can also affect the calculated results. For instance, the reported values of diffusion coefficient of Pb in Sn vary by a factor of 4 at similar compositions and temperatures. Furthermore, the assumptions that the partition coefficients and the liquidus slope are constants throughout the entire solidification range is quite inaccurate for some binary systems. All these uncertainties therefore must be considered when comparing experimental results to those calculated.

To date, HL is model has been validated in the literature only against experimental results concerning steady-state solidification and reasonable to good agreement has been reported.[35,39] A recent publication concerning solidification of Al-Cu alloys under steady-state conditions with a constant temperature gradient and a wide range of growth rates (9 to 490 μms^{-1}) has reported that the calculated results by the HL model are in good agreement with the experimental results for growth rates between 20 and 200 μms^{-1}.[39] However, for growth rates smaller than 20 μms^{-1} and higher than 200 μms^{-1}, significant discrepancies have been
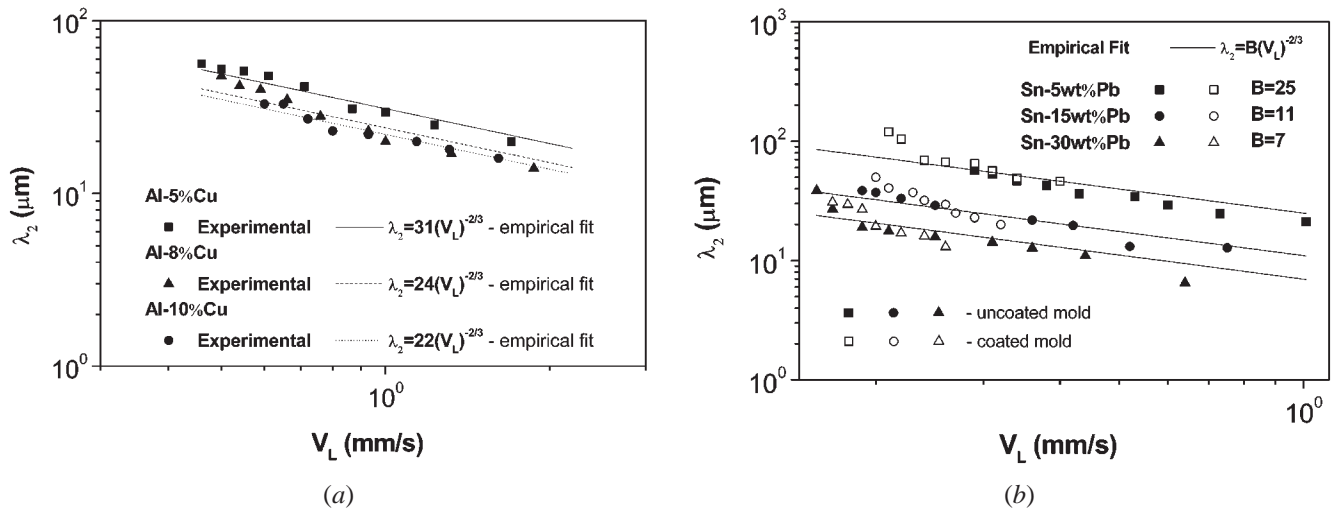
Fig. 9—Secondary dendrite arm spacing as a function of growth rate for (a) Al-Cu and (b) Sn-Pb alloys.

observed. This is the case of the present experimental investigation, *i.e.*, tip growth rates higher than 200 μms^{-1} but under unsteady-state heat flow conditions.

The BK model depends additionally on empirical dimensionless calibration parameters, a_1 for primary spacings and a_2 for secondary spacings, as shown by Eqs. [7] and [8]. These authors, based mainly on experimental results of a single article from the literature,[28] have proposed $a_1 = 250$ for Al alloys, $a_1 = 50$ for Sn alloys, and $a_2 = 5$ for Sn-Pb alloys.[29] For secondary spacings of Al-Cu alloys, they have proposed $a_2 = 5$ based on a wider range of experimental reports in the literature (including steady state), but in a recent publication concerning unsteady solidification, a more realistic value was found to be 7.4.[40] It is quite clear that additional experimental data would be required to ascertain the values of these calibration parameters, except for the latter case, which has been more extensively examined. This can explain the excellent agreement observed in Figure 15 between the theoretical predictions of BK's model ($a_2 = 7.4$) and the present experimental results concerning secondary spacings of Al-Cu alloys.

For steady-state growth, it has been claimed in the literature, for the majority of cases, that λ_1 increases as C_0 is increased. According to Spittle and Lloyd[46] under unsteady-state conditions, it may be possible that for a given value of $G_L \cdot V_L$, primary spacing can be smaller than the spacing that would be observed under steady-state growth for the same value of G_L and V_L. It is considered that unsteady-state solidification is initiated by chilling, which must inevitably induce supercooling in the liquid adjacent to the chill, to an extent that depends on C_0, and melt temperature. The initial spacing of primary arms therefore would presumably reflect the degree of undercooling in the liquid, and adjustment of this spacing to that value that would be observed under steady-state growth for similar conditions of G_L and V_L may be prevented by the high cooling rates.

In order to analyze the preceding statement, the present experimental results are compared in Figures 12 and 13 with the theoretical predictions furnished by the main predictive models existing in the literature, concerning the growth of primary spacings in steady-state conditions. These models have been validated in recent articles against experimental results of steady-state directional solidification of Sn-Pb[38]

and Al-Cu[39] alloys. For the Sn-Pb system, where the solute content has affected the primary spacings, it can be seen that, as a matter of fact, the experimental values obtained in unsteady-state conditions are smaller than those theoretically predicted by the steady-state models (Figure 12). On the other hand, for the Al-Cu system, where λ_1 was found to be independent of composition, the predictions furnished by the steady-state models have presented a fair to good agreement with the experimental results obtained under unsteady-state conditions, for all the compositions examined, as shown in Figure 13 (despite the high cooling rates observed in the early stages of the directional growth).

It is also important to remark that Al-Cu alloys are subjected to the inverse segregation phenomenon during vertical unidirectional solidification, which is responsible for higher solute concentrations at the bottom of castings because of the back flow of enriched liquid melt, and that could presumably have an influence on dendrite spacings. However, additional experiments for a wider range of alloys under unsteady-state solidification conditions are needed to fully understand the effect of the initial solute composition on primary spacings.

Because the unsteady-state theoretical models (HL and BK) have not furnished reliable predictions for primary spacings, the analytical expression for the cooling rate, given by Eq. [16], can be incorporated into the experimental equations shown in Figure 8, in order to establish empirical formulas permitting λ_1 to be expressed as a function of solidification parameters such as pouring temperature, type of mold, transient metal/mold heat-transfer coefficients, and metal/mold thermophysical characteristics, yielding

$$\lambda_1 = A \left\{ \left[\frac{m\Delta T_p}{\sqrt{\pi} \cdot \alpha_{SL}\phi_2[1 - \mathrm{erf}\,(m\phi_2)]\exp{(m\phi_2)^2}} \right] \right.$$

[19]

$$\left. \left[\frac{\dfrac{2\alpha_{SL}\phi_2^2}{2K_S\phi_2(T_{\mathrm{Sol}} - T_0)}}{n\sqrt{\pi}(T_{\mathrm{Liq}} - T_0)\exp{(\phi_1^2)}[M + \mathrm{erf}(\phi_1)]h_i} + S_L \right]^2 \right\}^{-0.55}$$
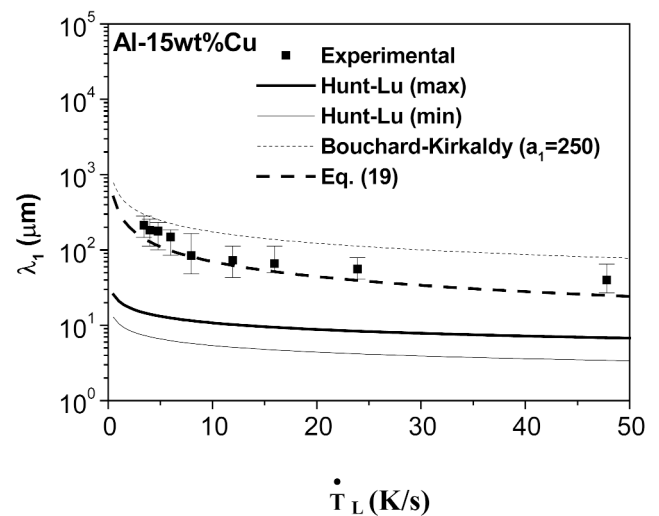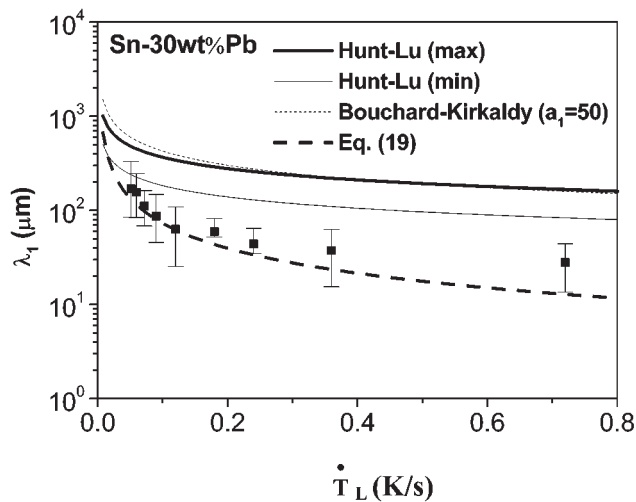
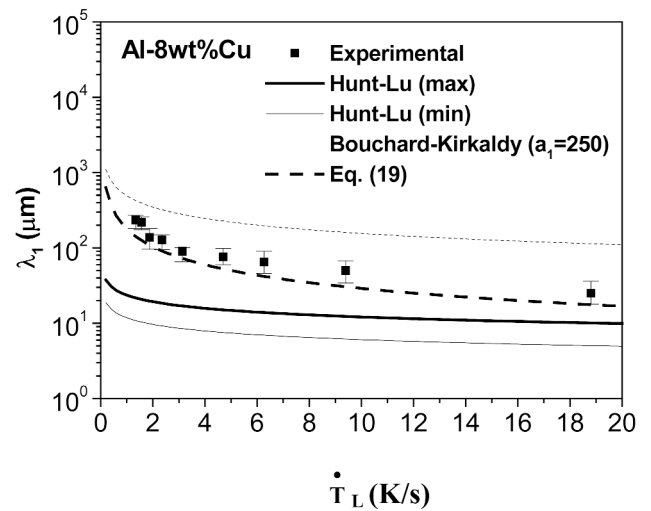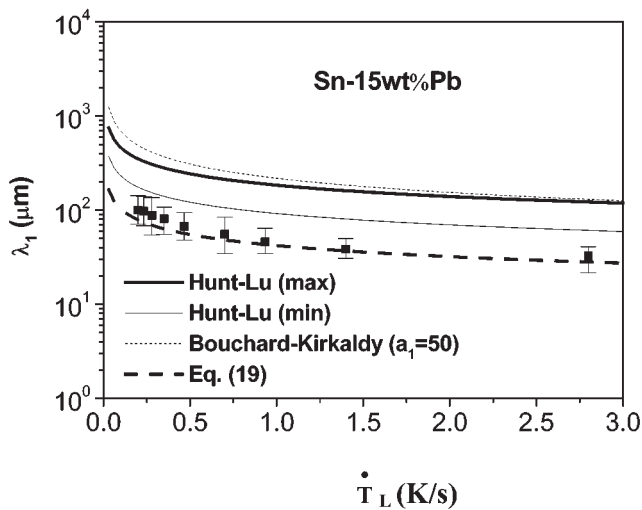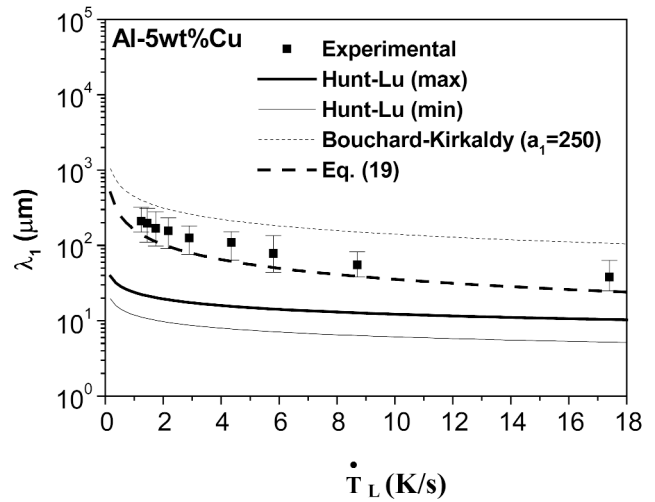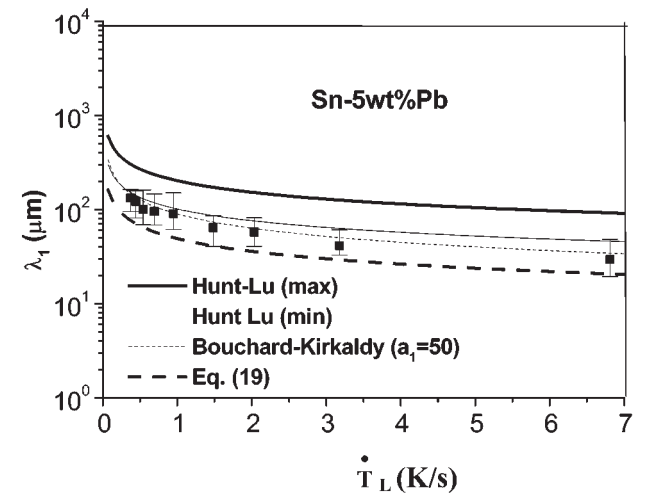Fig. 10—Comparison of experimental and theoretical primary dendrite arm spacings as a function of cooling rate for Sn-Pb alloys in unsteady-state directional solidification.

Fig. 11—Comparison of experimental and theoretical primary dendrite arm spacings as a function of cooling rate for Al-Cu alloys in unsteady-state directional solidification.

where

$A = 250$ for hypoeutectic Al-Cu alloys; and
$A = 80.5$ for Sn 5 wt pct Pb, $A = 44$ for Sn 15 wt pct Pb, and $A = 25$ for Sn 30 wt pct Pb alloys.

The predictions furnished by Eq. [19] are compared with experimental results in Figures 10 and 11, and a good agreement can be observed.
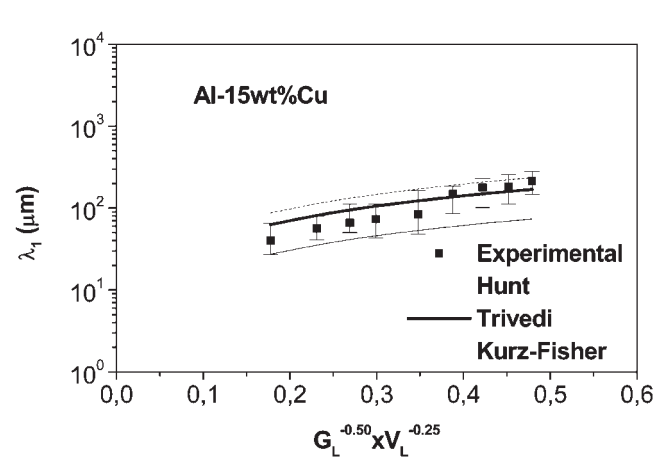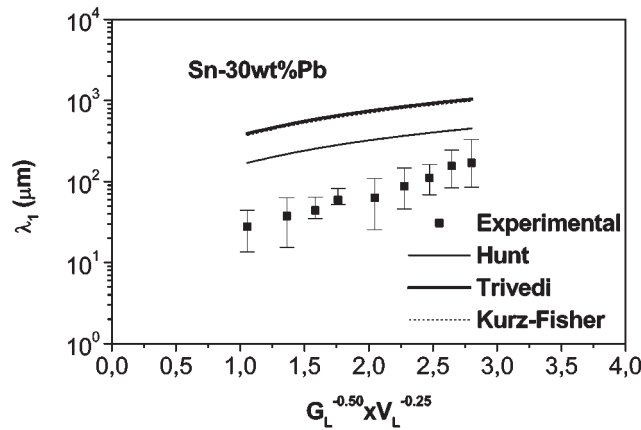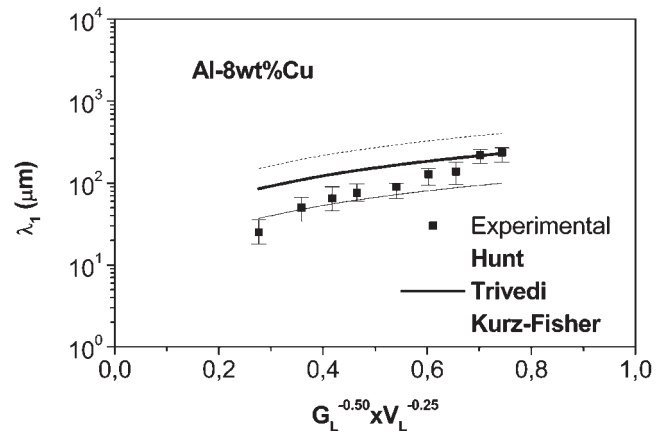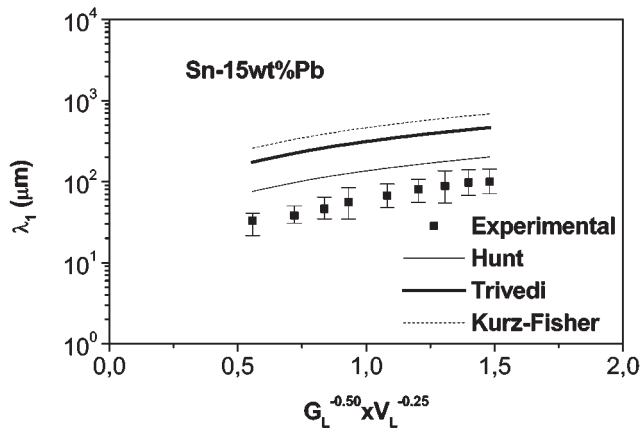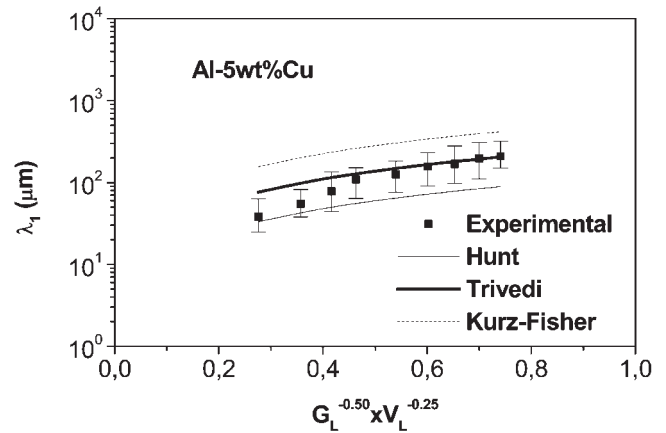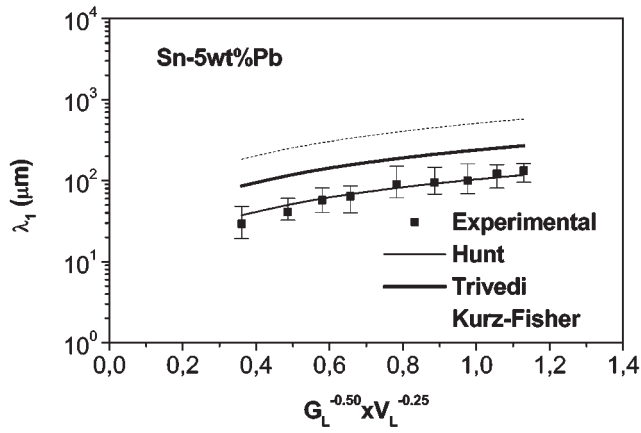
Fig. 12—Comparison of experimental (unsteady-state) and theoretical (steady-state) primary dendritic arm spacings for Sn-Pb alloys.

Fig. 13—Comparison of experimental (unsteady-state) and theoretical (steady-state) primary dendritic arm spacings for Al-Cu alloys.

Figures 14 and 15 illustrate the calculated and measured secondary dendrite arm spacings as a function of tip growth rate, for Sn-Pb and Al-Cu alloys, respectively. The theoretical approach was that due to Bouchard and Kirkaldy and represented by Eq. [8]. The used calibrating factors a_2 are those suggested by these authors for the Sn-Pb system[29] and that validated in a previous article for Al-Cu alloys.[40] It can be seen that a quite good agreement is observed between theory and experiment, for all alloys examined. The insertion of the analytical expression for tip growth rate into Eq. [8] will permit λ_2 to be

determined as a function of unsteady-state solidification parameters:

$$\lambda_2 = 2\pi a_2\left(\frac{4\Gamma D_L^2}{C_0(1 - k_0)^2 T_F}\right)^{1/3}$$

[20]

$$\left(\frac{2\alpha_{SL}\phi_2^2}{\left(\dfrac{2K_S\phi_2(T_{Sol} - T_0)}{n\sqrt{\pi}(T_{Liq} - T_0)\exp(\phi_1^2)[M + \text{erf}(\phi_1)]h_i}\right) + S_L}\right)^{-2/3}$$
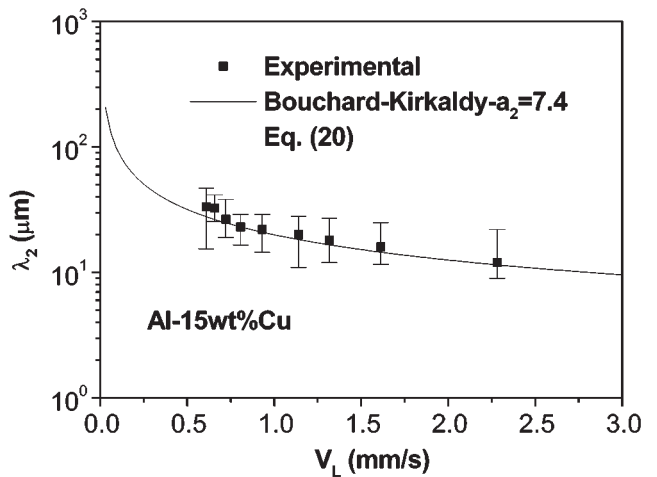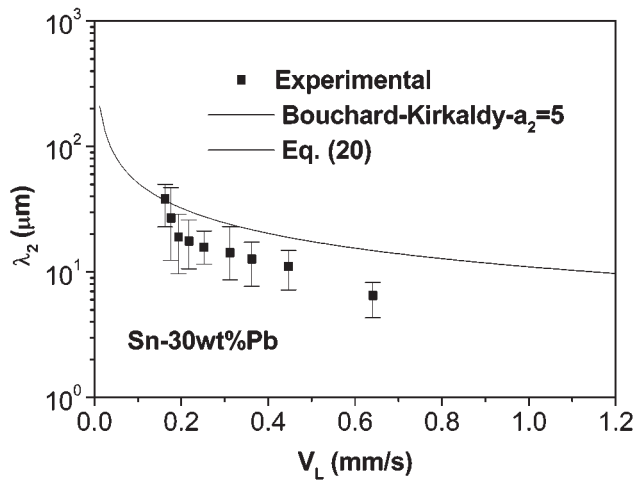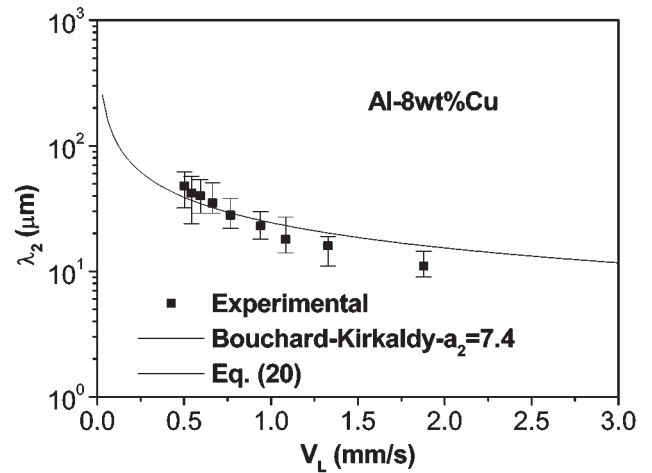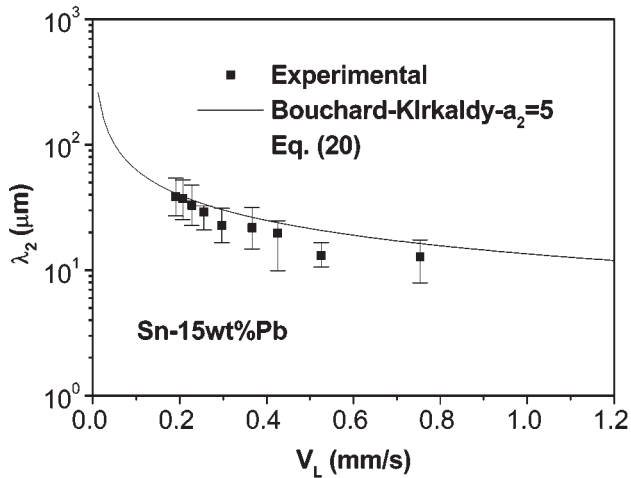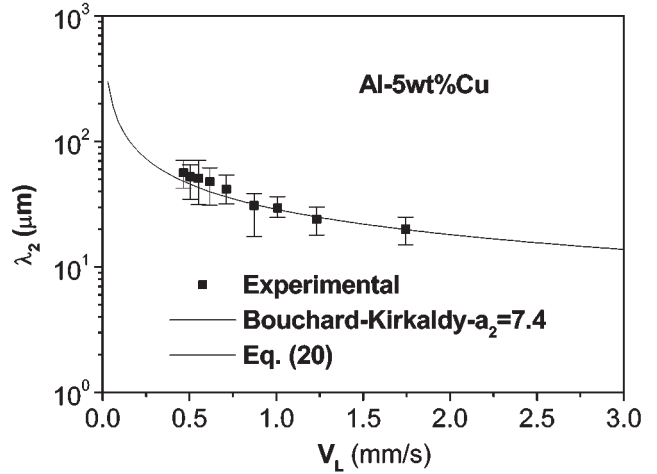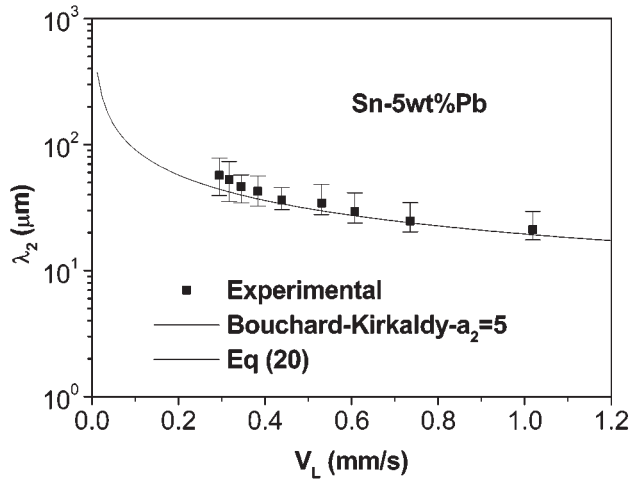
Fig. 14—Comparison of experimental and theoretical secondary dendrite arm spacings as a function of tip growth rate for Sn-Pb alloys.

Fig. 15—Comparison of experimental and theoretical secondary dendrite arm spacings as a function of tip growth rate for Al-Cu alloys.

where $a_2 = 5$ for Sn-Pb alloys and $a_2 = 7.4$ for Al-Cu alloys. Equation [20] is compared with experimental results and with predictions furnished by the BK model in Figures 14 and 15. It can be seen that no differences can be observed between the BK model and the empirical equation predictions.

V. SUMMARY

The following major conclusions are derived from the present study.

1. Under unsteady-state conditions, primary and secondary arm spacings were observed to decrease as the tip cooling

rate or the tip growth rate increased for a given Sn-Pb or Al-Cu alloy composition.

2. For Sn-Pb alloys solidified under unsteady-state conditions, both primary and secondary dendrite arm spacings decrease with increasing solute content. For Al-Cu alloys, the primary spacings were found to be independent of composition, and secondary spacings decrease as the solute content is increased.

3. The theoretical primary spacing models by HL and BK did not generate the experimental observations concerning the unsteady-state solidification of the Al-Cu and Sn-Pb alloys examined. The insertion of an analytical expression for cooling rate into the primary spacing experimental equations is proposed, in order to establish empirical formulas permitting λ_1 to be expressed as a function of solidification variables.

4. The theoretical BK's equation, relating secondary dendrite spacings with tip growth rate, has generated adequately the experimental results for both Al-Cu and Sn-Pb alloys directionally solidified in unsteady-state heat flow conditions. The insertion of an analytical expression for tip growth rate into BK's equation in order to establish empirical formulas permitting λ_2 to be expressed as a function of solidification variables is proposed.

5. The experimental primary arm spacings for the Sn-Pb alloys examined are smaller than those generated by the main theoretical steady-state growth models. For Al-Cu alloys, the experimental results agree reasonably well with the theoretical predictions furnished by these models.

ACKNOWLEDGMENTS

REFERENCES

1. J.D. Hunt: *Int. Conf. on Solidification and Casting of Metals*, The Metals Society, London, 1979, pp. 3-9.
2. W. Kurz and J.D. Fisher: *Acta Metall.*, 1981, vol. 29, pp. 11-20.
3. W. Kurz and J.D. Fisher: *Fundamentals of Solidification*, Trans Tech Publications, Aedermannsdorf, Switzerland, 1992, pp. 85-90.
4. J.D. Hunt and S.Z. Lu: *Metall. Mater. Trans. A*, 1966, vol. 27A, pp. 611-23.
5. V. Laxmanan: *Scripta Mater*, 1998, vol. 38, pp. 1289-97.
6. V. Laxmanan: *Acta Metall.*, 1985, vol. 33, pp. 1023-35.
7. V. Laxmanan: *Acta Metall.*, 1985, vol. 33, pp. 1037-49.
8. V. Laxmanan: *J. Cryst. Growth*, 1986, vol. 75, pp. 573-90.
9. L. Nastac: *Acta Mater.*, 1999, vol. 47, pp. 4253 to 62.
10. J.S. Kirkaldy and D. Venugopalan: *Scripta Metall.*, 1989, vol. 23, pp. 1603-08.
11. J.S. Kirkaldy, L.X. Liu, and A. Kroupa: *Acta Metall. Mater.*, 1995, vol. 43, pp. 2905-15.
12. J. Li, G. Yang, and Y. Zhou: *Mater. Res. Bull.*, 1998, vol. 33, pp. 141-48.
13. M.H. Burden and J.D. Hunt: *J. Cryst. Growth*, 1974, vol. 22, pp. 99-111.
14. R. Trivedi: *Acta Metall.*, 1970, vol. 18, pp. 287-96.
15. C.-A. Gandin, M. Eshelman, and R. Trivedi: *Metall. Mater. Trans. A.*, 1996, vol. 27 A, pp. 2727-39.
16. J.A. Warren and J.S. Langer: *Phys. Rev. A*, 1990, vol. 42, pp. 3518-25.
17. J.A. Warren and J.S. Langer: *Phys. Rev. E*, 1993, vol. 47, pp. 2702-12.
18. Q. Li and C. Beckermann: *Acta Mater.*, 1999, vol. 47, pp. 2345-56.
19. Q. Han, and J.D. Hunt: *Mater. Sci. Eng. A*, 1997, vol. 238, pp. 192-95.
20. B.J. Spencer and H.E. Huppert: *J. Cryst. Growth*, 1999, vol. 200, pp. 287-96.
21. R. Trivedi: *Metall. Mater. Trans. A*, 1984, vol. 15A, pp. 977-82.
22. R. Trivedi and W. Kurz: *Int. Mater. Rev.*, 1994, vol. 39, pp. 49-74.
23. T. Koseki and M.C. Flemings: *Iron Steel Inst. Jpn. Int.*, 1995, vol. 35, pp. 611-17.
24. D. Bouchard and J.S. Kirkaldy: *Metall. Mater. Trans. B*, 1996, vol 27B, pp. 101-13.
25. L. Makkonem: *J. Cryst. Growth*, 2000, vol. 208, pp. 772-78.
26. J.A. Horwarth and L.F. Mondolfo: *Acta Metall.*, 1962, vol. 10, pp. 1037-42.
27. J.O. Coulthard and R. Elliott: *J. Inst. Met.*, 1967, vol. 95, pp. 21-23.
28. T. Okamoto and K. Kishitake: *J. Cryst. Growth*, 1975, vol. 29, pp. 137-46.
29. D. Bouchard and J.S. Kirkaldy: *Metall. Mater. Trans. B*, 1997, vol. 28B, pp. 651-63.
30. D.G. McCartney and J.D. Hunt: *Acta Metall.*, 1981, vol. 29, pp. 1851-63.
31. M. Chen and T.Z. Kattamis: *Mater. Sci. Eng. A*, 1998, vol. 247, pp. 239-47.
32. B. Biblia, H. Jamgotchian, and L. Capella: *Acta Metall.*, 1981, vol. 29, pp. 1785-89.
33. C.T. Rios and R. Caram: *J. Cryst. Growth*, 1997, vol. 174, pp. 65-69.
34. B. Drevet, H. Nguyen Thi, D. Camel, B. Biblia, and M.D. Dupouy: *J. Cryst. Growth*, 2000, vol. 218, pp. 419-33.
35. J. Feng, W.D. Huang, X. Lin, Q.Y. Pan, T. Li, and Y.H. Zhou: *J. Cryst. Growth*, 1999, vol. 197, pp. 393-95.
36. X. Lin, W.D. Huang, J. Feng, T. Li, and Y. Zhou: *Acta Mater.*, 1999, vol. 47, pp. 3271-80.
37. L. Yu, G.L. Ding, J. Reye, S.N. Ojha, and S.N. Tewari: *Metall. Mater. Trans. A*, 1999, vol. 30A, pp. 2463-71.
38. E. Cadirli and M. Gündüz: *J. Mater. Sci.*, 2000, vol. 35, pp. 3837-48.
39. M. Gündüz and E. Çardili: *Mater. Sci. Eng. A*, 2002, vol. 327, pp. 167-85.
40. J.M.V. Quaresma, C.A. Santos, and A. Garcia: *Metall. Mater. Trans. A*, 2000, vol. 31A, pp. 3167-77.
41. X. Wan, Q. Han, and J.D. Hunt: *Acta Mater.*, 1997, vol. 45, pp. 3975-79.
42. M.F. Lima and H. Goldenstein: *J. Cryst. Growth*, 2000, vol. 208, pp. 709-16.
43. S. Yang, W. Huang, X. Lin, Y. Su, and Y. Zhou: *Scripta Mater.*, 2000, vol. 42, pp. 543-48.
44. R.M. Sharp and A. Hellawell: *J. Cryst. Growth*, 1969, vol. 5, pp. 155-61.
45. G.L. Ding, W.D. Huang, X. Huang, X. Lin, and H. Zhou: *Acta Mater.*, 1996, vol. 44, pp. 3705-09.
46. J.A. Spittle and D.M. Floyd: *Proc. Int. Conf. on Solidification and Casting of Metals*, The Metals Society, London, 1979, pp. 15-20.
47. S.M. Lee, K.A.Q. O'Reilly, B. Cantor, and C.P. Hong: *Mater. Sci. Eng. A*, 1998, vol. 49, pp. 233-40.
48. J. Lapin, A. Klimová, R. Velisek, and M. Kursa: *Scripta Mater.*, 1997, vol. 37, pp. 85-91.
49. N. Tiedje, P.N. Hansen, and A.S. Pedersen: *Metall. Mater. Trans. A*, 1996, vol. 27, pp. 4085-93.
50. M. Lin, T. Mori, and H. Iwasaki: *Mater. Sci. Eng. A*, 1999, vol. 265, pp. 217-23.
51. S.P. O'Dell, G.L. Ding, and S.N. Tewari: *Metall. Mater. Trans. A*, 1999, vol. 30A, pp. 2159-65.
52. L.X. Liu and J.S. Kirkaldy: *Acta Metall. Mater.*, 1995, vol. 43, pp. 2891-904.
53. G. Ding, W. Huang, X. Lin, and Y. Zhou: *J. Cryst. Growth*, 1997, vol. 177, pp. 281-88.
54. V.L. Voller and C.R. Swaminathan: *Num. Heat Tranfer B*, 1991, vol. 19, pp. 175-89.
55. W.R. Osório and A. Garcia: *Mater. Sci. Eng. A*, 2002, vol. 325, pp. 104-12.
56. C.A. Santos, J.M.V. Quaresma, and A. Garcia: *J. Alloys Compounds*, 2001, vol. 319, pp. 174-86.
57. W.W. Mullins and R.F. Sekerka: *J. Appl. Phys.*, 1965, vol. 35(1), pp. 264-68.
58. W.W. Mullins and R.F. Sekerka: *J. Appl. Phys.*, 1965, vol. 36(2), pp. 444-51.
59. C.A. Siqueira, N. Cheung, and A. Garcia: *Metall. Mater. Trans. A*, 2002, vol. 33A, pp. 2107-2118.